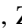# Long and Short Fast Radio Bursts Are Different from Repeating and Nonrepeating Transients

X. J. Li[1], X. F. Dong[1], Z. B. Zhang[1] , and D. Li[2,3]

[1] School of Physics and Physical Engineering, Qufu Normal University, Qufu 273165, People's Republic of China; z_b_zhang@sina.com
[2] National Astronomical Observatories, Chinese Academy of Sciences, Beijing 100101, People's Republic of China; dili@nao.cas.cn
[3] NAOC-UKZN Computational Astrophysics Centre, University of KwaZulu-Natal, Durban 4000, South Africa
Received 2021 July 23; revised 2021 October 10; accepted 2021 October 14; published 2021 December 24

Abstract

We collect 133 fast radio bursts (FRBs), including 110 nonrepeating and 23 repeating ones, and systematically investigate their observational properties. To check the frequency dependence of FRB classifications, we define our samples with a central frequency below/above 1 GHz as subsample I/II. First, we find that there is a clear bimodal distribution of pulse width for subsample I. If we classify FRBs into short FRBs (sFRBs; <100 ms) and long FRBs (lFRBs; >100 ms) as done for short and long gamma-ray bursts (GRBs), the sFRBs at higher central frequency are commonly shorter than those at lower central frequency not only for nonrepeating but also repeating sFRBs. Second, we find that fluence and peak flux density are correlated with a power-law relation of $F \propto S_{p,\mathrm{obs}}^{\gamma}$ for both sFRBs and lFRBs whose distributions are obviously different. Third, the lFRBs with isotropic energies ranging from 10^{42} to 10^{44} erg are more energetic than the sFRBs in the F–DM_{EX} plane, indicating that they are two representative types. Finally, it is interesting to note that the peak flux density behaves independently on the redshift when the distance of the FRBs becomes far enough, which is similar to the scenario of the peak flux evolving with redshift in the field of GRBs. We predict that fainter FRBs at a higher redshift of $z > 2$ can be successfully detected by FAST and the Square Kilometre Array in the near future.

Unified Astronomy Thesaurus concepts: Radio bursts (1339); High energy astrophysics (739); Radio transient sources (2008); Extragalactic radio sources (508); Radio continuum emission (1340)

1. Introduction

Fast radio bursts (FRBs) discovered by the Parkes 64 m telescope for the first time are transient radio pulses of millisecond durations that flash randomly in the sky (Lorimer et al. 2007; Thornton et al. 2013). Their isotropic peak luminosities are widely distributed from about 10^{38} erg s^{-1} to 10^{46} erg s^{-1}, and the typical isotropic energies vary from about 10^{35} erg to 10^{43} erg (Zhang 2018a, 2020a).

FRB 121102 as the first repeater was reported by Spitler et al. (2016), and 10 repeating bursts were discovered by Arecibo Observatory subsequently. Then, Scholz et al. (2016) detected six follow-up bursts from this source: five bursts with the Green Bank Telescope (GBT) at 2 GHz, and one at 1.4 GHz with the Arecibo Observatory. Until now, FRB 121102 has been found to reburst a few thousand times (Li et al. 2019, 2021). In 2018, the Canadian Hydrogen Intensity Mapping Experiment (CHIME; CHIME/FRB Collaboration et al. 2018) reported the second source of repeating FRB 180814.J0422+73 (CHIME/FRB Collaboration et al. 2019a). Currently, there are already about two dozen repeaters published in the literature (see Table 1 of this work). As the number of repetitions increases, some statistical studies of the observational properties of these repeating bursts have been conducted. For instance, it is found that the waiting time distribution of FRB 121102 shows a clear bimodal distribution and does not correlate with the burst intensity, suggesting some external mechanisms for these repeating bursts (Li et al. 2019; Sun et al. 2021). Furthermore, Kumar et al. (2019)

detected two repetitions of FRB 171019 with GBT, the brightness of which is a factor of ∼590 fainter than the first detection of FRB 171019 in the Australian Square Kilometre Array Pathfinder (ASKAP) fly's eye survey (Shannon et al. 2018). Meanwhile, Luo et al. (2020) carried out four follow-up observations of FRB 180301 first discovered by the Parkes radio telescope (Price et al. 2019), using the Five-hundred-meter Aperture Spherical radio Telescope (FAST; Li et al. 2018), and found 15 repetitions from FRB 180301. Clearly, whether all FRBs repeat is an open question. In particular, a few previous "nonrepeating" FRBs have been identified to be repeating events. Therefore, restudying the statistical features of FRBs with a complete sample becomes more and more urgent and necessary.

At present, various progenitor models are proposed to explain FRBs, most of which involve compact objects (Platts et al. 2019).[4] Some source models are catastrophic and can only be applied to explain nonrepeating FRBs, such as the mergers or interactions of compact binaries (Kashiyama et al. 2013; Totani 2013; Mingarelli et al. 2015; Bhattacharyya 2017; Dong et al. 2018), collapse of compact objects (Falcke & Rezzolla 2014; Zhang 2014), and collisions of asteroids with neutron stars (Geng & Huang 2015; Huang & Geng 2016). After repeating FRB 121102 was detected, many models for repeating FRBs have been developed. A leading model for repeating FRBs is extragalactic magnetars (Lyubarsky 2014; Beloborodov 2017; Metzger et al. 2019). In addition, Gu et al. (2016) reported that the interaction between the bipolar magnetic fields of a neutron star and a magnetic white dwarf can be considered as a possible origin of repeating FRBs. Dai et al. (2016) proposed that a strongly magnetized NS encountering an extragalactic asteroid belt (EAB) around a stellar-mass object can arise as a repeating

---

[4] https://frbtheorycat.org

Table 1
Parameters of the First-detected Events for the 23 Repeating FRBs

No.	FRB	DM (pc cm^{-3})	S/N	z	$W_{\rm obs}$ (ms)	$S_{p,\rm obs}$ (Jy)	F (Jy ms)	Ref.
1	20200120E	87.782 ± 0.003	22.9	<0.03	0.16 ± 0.05	1.8 ± 0.9	2.25 ± 0.12	[1]
2	190907.J08 + 46	310.0 ± 0.4	10[e]	0.21	3 ± 1	1.7 ± 0.6	0.3 ± 0.2	[2]
3	190604.J1435 + 53	552.6 ± 0.2	33.8[e]	0.43	3 ± 0.4	0.9 ± 0.4	8.3 ± 2.8	[2]
4	190417.J1939 + 59	1378.1 ± 0.2	13.4[e]	1.08	3.3 ± 0.9	4.4 ± 0.8	0.5 ± 0.2	[2]
5	190303.J1353 + 48	221.8 ± 0.5	11.2[e]	0.16	2.0 ± 0.3	0.5 ± 0.3	2.3 ± 0.9	[2]
6	190222.J2052 + 69	460.6 ± 0.1	31.2[e]	0.31	2.97 ± 0.9	1.9 ± 0.6[a]	7.5 ± 2.3	[3]
7	190212.J18 + 81	301.7 ± 0.3	9.9[e]	0.21	4.1 ± 1.6	0.4 ± 0.3	3.0 ± 1.5	[2]
8	190213.J02 + 20	651.1 ± 0.4	9.9[e]	0.51	10 ± 2	0.06 ± 0.03[d]	0.6 ± 0.3	[2]
9	190209.J0937 + 77	424.6 ± 0.6	11.8[e]	0.32	3.7 ± 0.5	0.4 ± 0.2[a]	2.0 ± 1.0	[3]
10	190208.J1855 + 46	579.9 ± 0.2	12.2[e]	0.42	0.91 ± 0.16	1.4 ± 0.6	0.4 ± 0.2	[2]
11	190117.J2207 + 17	393.3 ± 0.1	24.2[e]	0.29	1.44 ± 0.03	1.7 ± 0.6	5.9 ± 1.6	[2]
12	190116.J1249 + 27	444.0 ± 0.6	12.9[e]	0.35	4.0 ± 0.5	0.3 ± 0.2[a]	0.8 ± 0.4	[3]
13	181128.J0456 + 63	450.2 ± 0.3	23.4[e]	0.28	2.43 ± 0.16	0.5 ± 0.3[a]	4.4 ± 2.2	[3]
14	181119.J12 + 65	364.2 ± 1.0	11.1[e]	0.28	6.3 ± 0.6	0.3 ± 0.2[a]	1.8 ± 0.8	[3]
15	181030.J1054 + 73	103.5 ± 0.7	11.5[e]	0.05	0.59 ± 0.08	3.2 ± 1.7[a]	7.3 ± 3.8	[3]
16	181017.J1705 + 68	1281.9 ± 0.4	12.9[e]	1.03	13.4 ± 1.4	0.4 ± 0.3[a]	1.0 ± 0.5	[3]
17	180916.J0158 + 65	349.2 ± 0.4	18.7[e]	0.12	1.40 ± 0.07	1.4 ± 0.06[a]	2.3 ± 1.2	[3]
18	180908.J1232 + 74	195.7 ± 0.9	10.4[e]	0.13	1.91 ± 0.1	0.6 ± 0.4	2.7 ± 1.1	[2]
19	180814.J0422 + 73	189.38 ± 0.1	24	0.09	2.6 ± 0.2	8.08 ± 5.80[d]	21 ± 15	[4]
20	180301	522 ± 5	20	0.37	2.18 ± 0.06	1.2 ± 0.1	1.3	[5]
21	171019	460.8 ± 1.1	23.4	0.35	5.4 ± 0.3	40.5[c]	219 ± 5	[6]
22	121102	557.4 ± 2.0	14	0.31	3.0 ± 0.5	$0.4^{+0.4}_{-0.2}$	$1.2^{+1.6}_{-0.55}$	[7]
23	151125[b]	273 ± 4	8.5	0.19	1680 ± 40[c]	0.54	2450	[8]

Notes. References: [1] Bhardwaj et al. (2021); [2] Fonseca et al. (2020); [3] CHIME/FRB Collaboration et al. (2019b); [4] CHIME/FRB Collaboration et al. (2019a); [5] Price et al. (2019); [6] Shannon et al. (2018); [7] Spitler et al. (2016); [8] Fedorova & Rodin (2019b).
[a] The parameters are not given in the FRB Catalog (https://frbcat.org) but are given in the literature.
[b] A very long repeating *l*FRB.
[c] The parameter is not given in the literature but is given in the FRB Catalog.
[d] These values are estimated with $F = S_{p,\rm obs} \times W_{\rm obs}$.
[e] These parameters are not reported in both the literature and the FRB Catalog but are reported in the CHIME/FRB Catalog 1 (https://www.chime-frb.ca/catalog).

FRB (Dai 2020). Besides, there are also other models, for example, neutron star cosmic combs (Zhang 2017, 2018b) and young rapidly rotating pulsars that can also lead to repeating FRBs (Lyutikov et al. 2016). Very recently, Geng et al. (2021) proposed that the repeating FRBs can be produced by the intermittent fractional collapses of the crust of a strange star and the 16 day periodicity of FRB 180916.J0158+65 can be well interpreted.

The observed spectral–temporal differences support the different origins between repeating and nonrepeating FRBs. Generally, the pulses of nonrepeating FRBs are shorter in duration than those of repeating FRBs (Scholz et al. 2016; CHIME/FRB Collaboration et al. 2019b; Fonseca et al. 2020). Compared to nonrepeating FRBs, repeating FRBs show complex subpulse frequency structure and drifting and spectral variation (CHIME/FRB Collaboration et al. 2019a). Polarimetric measurements exhibit diversity, including a constant polarization angle for some repeating FRBs or variable polarization angles for some nonrepeating FRBs (Masui et al. 2015; Michilli et al. 2018; CHIME/FRB Collaboration et al. 2019b; Cho et al. 2020; Luo et al. 2020). How the FRBs populate is always one of the most exciting open questions. Considering the above controversial results, we expand the FRB samples to include the latest FRBs published in recent papers in order to disclose the nature of these radio transients in statistics reliably and systematically. Using a larger repeating FRB sample, we deeply explore the possible observational differences between repeating and nonrepeating FRBs. It is worth pointing out that we define the short and long

FRBs, and compare their observational parameters for the first time in this work. In addition, we examine the detectability of FRBs by different radio telescopes at higher redshift. The sample selection and data preparation are given in Section 2. The results are presented in Section 3. Finally, we summarize and discuss the results in Section 4.

2. Data and Method

Our sample comprises 133 FRBs, of which 129 FRBs are taken from the database of FRB Catalog (published up to 2020 July; refer to Petroff et al. 2016), a nearby repeating FRB 20200120E on the outskirts of M81 was detected by CHIME (Bhardwaj et al. 2021), and three new nonrepeating FRBs, 181017.J0036+11, 181118, and 181130, were reported by FAST (Niu et al. 2021). In total, there are 110 nonrepeating FRBs and 23 repeating FRBs (including 116 repeaters) in our samples. Table 1 lists the first pulses of 23 repeating FRBs with the observed width ($W_{\rm obs}$), redshift (z), dispersion measure (DM), peak flux density ($S_{p,\rm obs}$), fluence (F), and the references therein.

Generally, the total DM of an FRB at redshift z is contributed by four components, i.e.,

$$DM = DM_{\rm MW} + DM_{\rm EX}$$

$$= DM_{\rm MW} + DM_{\rm IGM} + \frac{DM_{\rm host} + DM_{\rm src}}{1 + z}, \quad (1)$$

where $DM_{\rm EX}$ is an excess of DM with respect to the Milky Way value of $DM_{\rm MW}$, the subscripts MW, IGM, host, and src refer
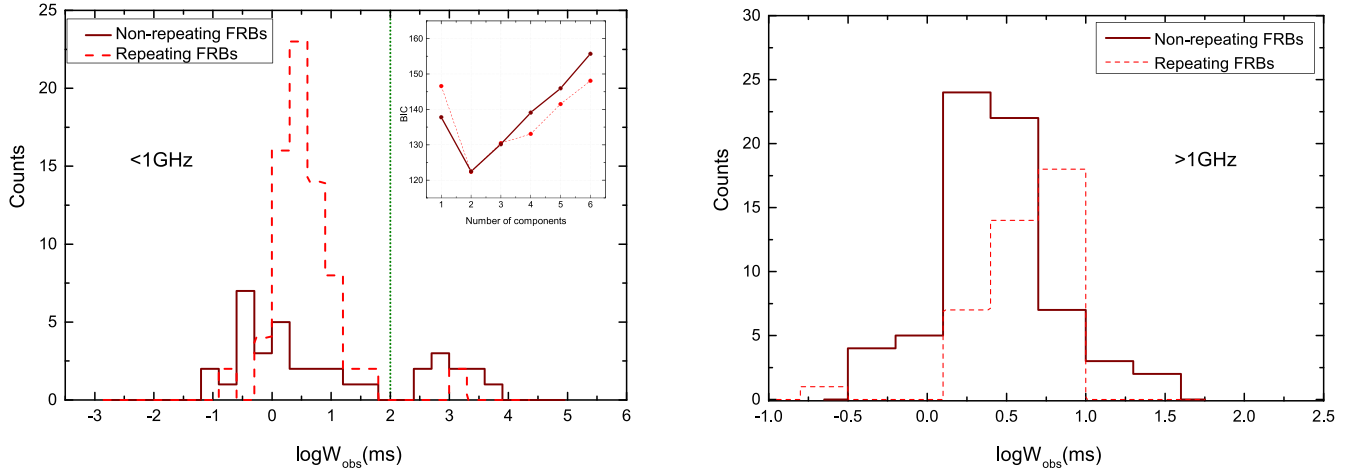
Figure 1. Distributions of W_{obs} for nonrepeating bursts (solid) and repeating bursts (dashed) detected at a central frequency below 1 GHz (left panel) and above 1 GHz (right panel). Short and long FRBs are divided by the dotted green vertical line at $W_{obs}=100$ ms phenomenologically. The insert in the left panel shows the inferred BIC values versus the number of components.

to the contributions of the plasma from the Milky Way, intergalactic medium, FRB host galaxy, and source environment, respectively (Zhang 2018a; Xiao et al. 2021).

The isotropic peak luminosity and isotropic energy of an FRB at a central frequency of ν_c from Zhang (2018a) can be calculated as

$$L_p \simeq 4\pi D_L^2 S_{\nu,p}\nu_c$$
$$= \left(10^{42}\mathrm{ergs}^{-1}\right)4\pi\left(\frac{D_L}{10^{28}\ \mathrm{cm}}\right)^2 \frac{S_{\nu,p}}{\mathrm{Jy}}\ \frac{\nu_c}{\mathrm{GHz}}, \qquad (2)$$

$$E \simeq \frac{4\pi D_L^2}{1+z}F_\nu\nu_c$$
$$= \left(10^{39}\mathrm{erg}\right)\frac{4\pi}{1+z}\left(\frac{D_L}{10^{28}\ \mathrm{cm}}\right)^2 \frac{F_\nu}{\mathrm{Jy}\cdot\mathrm{ms}}\ \frac{\nu_c}{\mathrm{GHz}}, \qquad (3)$$

where $S_{\nu,p}$ is the specific peak flux density (in units of Jy), F_ν is the fluence (in units of Jy ms), D_L is the luminosity distance (in units of cm), and ν_c is the central frequency (in units of GHz). It is worth noting that Aggarwal (2021) argued that a bandwidth other than the central frequency should be utilized to estimate the isotropic energies of repeating FRBs in particular (see also Petroff et al. 2016). We nonetheless use the central frequency as the parameter since the majority of FRB samples detected by multiple telescopes within different bandwidths are nonrepeating ones currently. Throughout this paper, a flat ΛCDM universe with $\Omega_m = 0.286$, $\Omega_\Lambda = 0.714$, and $H_0 = 69.6$ km s^{-1} Mpc^{-1} has been assumed (Bennett et al. 2014).

3. Results

3.1. Pulse Width

There are 103 nonrepeating and 111 pulses for 23 repeating FRBs with the width measured. A Kolmogorov–Smirnov test to repeaters and nonrepeaters returns the statistic $D = 0.22$ and $P = 0.01$ for the W_{obs} distributions. If adopting a critical value $D_\alpha = 0.19$ at a significance level of $\alpha = 0.05$, one can conclude that the width distributions of repeating FRBs are somewhat different from nonrepeating ones.

To check the frequency dependence of FRB classifications, we define the FRBs with a central frequency below 1 GHz as subsample I and the FRBs with a central frequency above 1 GHz to be subsample II, temporally. In Figure 1, the left panel shows the W_{obs} distributions of subsample I at lower frequency and the right panel shows for the subsample II at higher frequency. Then, we perform the maximum-likelihood (ML) analysis along with Gaussian mixture model (GMM) to find the number of components in terms of the Bayesian information criterion (BIC) for subsample I with PYTHON machine learning package SCIKIT-LEARN (Pedregosa et al. 2011). The BIC value is plotted against the component number in the inset of the left panel like some previous works (Kass & Raftery 1995; Tarnopolski 2016; Zhang et al. 2016). It is interestingly found that the BIC curves of distinct kinds of FRBs always reach the smallest value at the point of two components. Additionally, the BIC differences between one and two components are $\triangle$ BIC = 15 and 24 for nonrepeating and repeating FRBs, respectively. This evidently demonstrates that the lognormal widths of both nonrepeating and repeating FRBs in our lower (unlike our higher) frequency sample are bimodally distributed. Motivated by the similarity to the duration distributions of GRBs, we separate FRBs into two classes, that is, short FRBs (sFRBs) with a duration less than 100 ms and long FRBs (lFRBs) with a duration longer than 100 ms. It is found that there is no lFRB events in subsample II. The average W_{obs} of the repeating and nonrepeating sFRBs are $5.74^{+0.17}_{-0.17}$ ms and $4.53^{+0.45}_{-0.37}$ ms in subsample I ($4.60^{+0.09}_{-0.01}$ ms and $3.96^{+0.21}_{-0.15}$ ms in subsample II), respectively. The average W_{obs} of 10 nonrepeating lFRBs is 1698 ± 11.31 ms. For the two bursts of repeating lFRB 151125, the values of W_{obs} are 1680 ± 40 ms and 1470 ± 40 ms, comparable to the average value of nonrepeating lFRBs. As a whole, the duration of lFRBs is about three orders of magnitude longer than that of sFRBs for both repeating and nonrepeating FRBs. Note that all lFRBs except 151125 are "one-off" events in our sample.

In addition, we find that the pulses in nonrepeating sFRBs are narrower than those in repeating ones not only at higher frequency but also at lower frequency as shown in Figure 1. However, the result of lFRBs is ambiguous, which is likely biased by a small number of lFRBs especially for nonrepeating lFRBs. Interestingly, the ultralong radio pulses with a duration
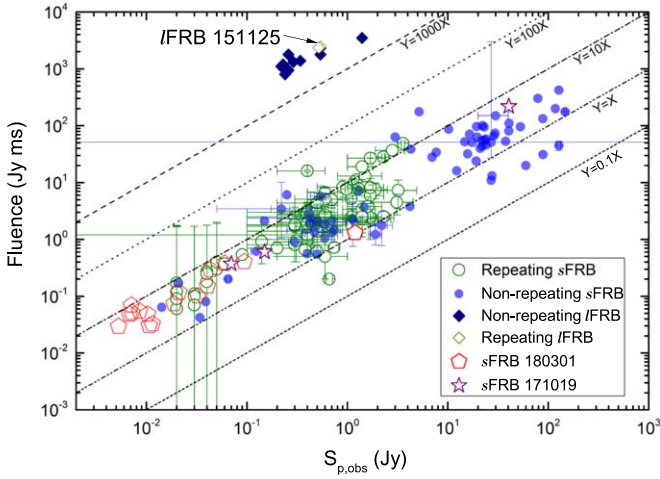
Figure 2. Fluence is plotted against $S_{p,\mathrm{obs}}$. Five ratios of fluence to $S_{p,\mathrm{obs}}$ are symbolized by the dashed, dotted, dashed–dotted, dashed–dotted–dotted, and short-dashed lines for 1000, 100, 10, 1, and 0.1, respectively.

Table 2
The Best-fit Parameters of the Correlations between $S_{p,\mathrm{obs}}$ and Fluence for All Kinds of FRBs

FRB	γ	μ	ρ^{a}
Nonrepeating sFRBs	0.86 ± 0.04	0.52 ± 0.05	0.92
Repeating sFRBs	0.95 ± 0.06	0.60 ± 0.04	0.87
All sFRBs	0.86 ± 0.03	0.55 ± 0.03	0.92
All lFRBs	0.71 ± 0.12	3.50 ± 0.06	0.88

Note.
[a] Pearson correlation coefficient.

of 1–2 s have been merely detected at a lower frequency of <1 GHz. Furthermore, we find that nonrepeating sFRBs with a higher central frequency are shorter than those of nonrepeating ones with a lower central frequency, as do repeating sFRBs, similar to the conclusion reported by Gajjar et al. (2018) and Josephy et al. (2019), indicating the scatter-broadening phenomenon when the signal propagates through the interstellar medium (Xu & Zhang 2016; Nikitin 2021).

3.2. The Densities of Flux and Fluence

Figure 2 shows that nonrepeating sFRBs typically have a higher brightness than repeating bursts on average. However, the distributions of their intensities overlap each other. Meanwhile, it is found that the range of nonrepeating sFRBs is wider than that of repeating bursts, and the intensities of repeating FRBs are relatively lower. In Figure 2, it is noticeable that two repeating sFRBs 171019 (purple stars) and 180301 (red pentagons) had been incorrectly indicated to be one-off events. Follow-up observations indicate that their radiative intensities became fainter and fainter since the first pulse. Considering the two special FRBs without fluence reported in the FRB Catalog and the literature, we have chosen the relation $F = S_{p,\mathrm{obs}} \times W_{\mathrm{obs}}$ (Petroff et al. 2016) to estimate the unknown fluences.

Unlike before, we propose a power-law correlation of $F = \mu S_{p,\mathrm{obs}}^{\gamma}$ to apply to all kinds of FRBs. Table 2 lists our best-fitting results and correlation coefficients. The results demonstrate that the power-law relations exist in all kinds of FRBs with a roughly consistent power-law index of $\gamma \sim 0.9$. However, the intercept of
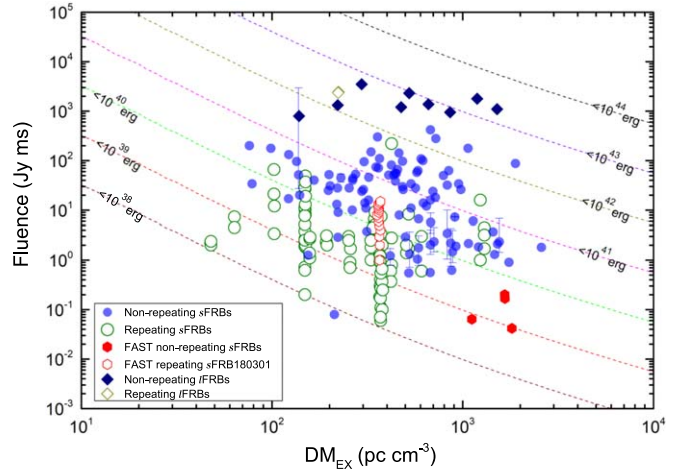

Figure 3. The fluence–DM_{EX} diagram. The dashed curves labeled with individual numbers stand for the upper limits of radio isotropic energies of FRBs from Equation (3).

the F–$S_{p,\mathrm{obs}}$ relations of lFRBs and sFRBs are obviously different. Figure 2 also shows that most sFRBs are located in the region of $F \sim (1 - 10)S_{p,\mathrm{obs}}$. It is surprisingly found that the lFRBs lie in the area of $F > 10^3 S_{p,\mathrm{obs}}$ and they violate the F–$S_{p,\mathrm{obs}}$ relation of sFRBs in evidence. Very interestingly, the repeating lFRB 151125 is consistent with those nonrepeating lFRBs, which may hint that some one-off lFRBs currently could be subsequently repetitive.

3.3. Fluence versus Dispersion Measure

Figure 3 shows that the updated fluence–DM_{EX} relation after the lFRBs and some new bursts are added. Note that DM_{EX} equals DM_{IGM} under the assumptions of $DM_{\mathrm{host}} = 0$ and $DM_{\mathrm{src}} = 0$. A rough relation $z \sim DM_{\mathrm{IGM}}/855\ \mathrm{pc\ cm}^{-3}$ was used to estimate the redshift of an FRB (Zhang 2018a). A higher fluence range of the lFRB samples can be distinguished clearly. Given the sFRB samples, our result is basically consistent with those of Shannon et al. (2018) and Niu et al. (2021).

In Figure 3, it also can been found that the energies of all FRBs span a broader range from $\sim 10^{38}$ to 10^{44} erg than those given by Luo et al. (2020) and Niu et al. (2021). The main reason is that the lFRBs with higher fluence (or isotropic energy) but comparable redshift have been included in this study. Besides, we added four new FRBs, including FRBs 181123, 181130, 181118, and 181017.J0036+11, with much lower fluences and larger DM_{EX} measurements detected by FAST (Zhu et al. 2020; Niu et al. 2021). It is excitingly found that the repeating sFRBs/lFRBs in our samples are less energetic than nonrepeating sFRBs/lFRBs on the whole. In particular, FRB 121102 has an isotropic energy less than 10^{40} erg that is good in agreement with Li et al. (2021). More excitingly, we find from Figure 3 that the isotropic energies of lFRBs are at least two orders of magnitude larger than those of sFRBs. This is quite similar to the energetic difference between short and long GRBs (e.g., Zhang et al. 2018a).

3.4. Peak Flux Density versus Redshift

In Figure 4, we study the redshift dependence of the peak flux densities of FRBs based on our samples. We display the evolution profiles of the peak flux density versus redshift for different telescopes. The isotropic peak luminosity can be determined from $L_p = 4\pi D_l^2(z) S_{p,\mathrm{obs}}(z)\nu_c k$ with a K-correction
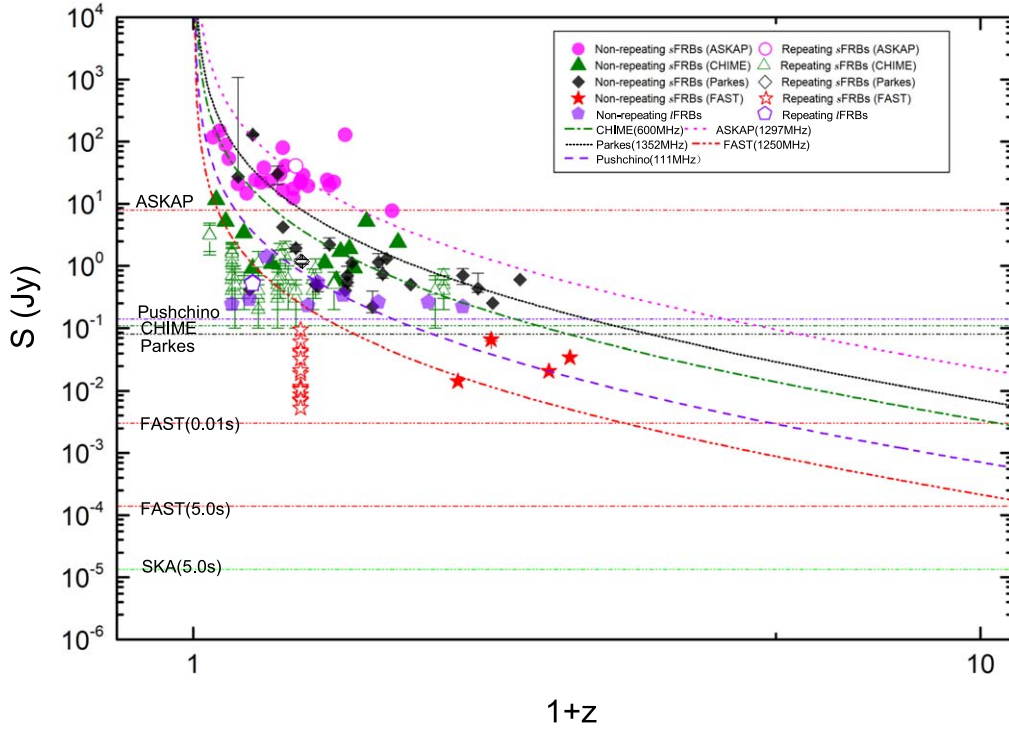
Figure 4. Peak flux density vs. redshift for FRBs detected by different telescopes. The slanted curves are plotted for the flux densities evolving with the redshift with an additional negative K-correction effect. The sensitivity limits of the different telescopes are marked by different horizontal lines. In particular, two sensitivity lines of FAST are given for $\Delta\tau = 10$ ms and $\Delta\tau = 5.0$ s. The green dotted–dotted–dashed horizontal line represents the sensitivity of SKA at $\Delta\nu = 700$ MHz and $\Delta\tau = 5$ s.

factor of $k = (1 + z)^{\alpha - \beta}$, where $\alpha \sim 0$ and $\beta \sim 1/3$ are the normal temporal and spectral indices defined in $S_\nu(t) \propto t^\alpha \nu^\beta$ (Soderberg et al. 2004; Chandra & Frail 2012; Zhang et al. 2018b).

The sensitivity of different telescopes can be estimated by the equation (Zhang et al. 2015; Caleb et al. 2016)

$$S_{\nu,\text{limt}} = \frac{\beta T_{\text{sys}} S/N}{G\sqrt{\Delta\nu \Delta\tau N_p}}, \qquad (4)$$

where T_{sys} is the system temperature in units of K, S/N is the signal-to-noise ratio, β is the digitization factor, G is the system gain in K Jy^{-1}, $\Delta\nu$ is the bandwidth in units of Hz, $\Delta\tau$ is the integration time in unit of seconds, and N_p is the number of polarizations. Note that in the FRB catalog the S/N values of lFRBs ranging from 7.3 to 10.1 are considerably smaller than those of the majority of sFRBs. The S/N differences in burst-detection significance may influence the transparency of our results in a sense. For example, if we apply an S/N threshold of 10 to our analysis, most lFRBs would be likely excluded from our sample due to their relatively lower significance level of S/N. According to Deng et al. (2019) and Josephy et al. (2019), the fluence threshold limits are 2 Jy ms, 51 Jy ms, and 7 Jy ms, respectively, for Parkes, ASKAP, and CHIME. In our samples, the maximum pulse widths are 25 ms for Parkes FRB 010312, 6.5 ms for ASKAP FRB 190711, and 63 ms for CHIME FRB 180814.J0422+73. Therefore, one can determine the detection thresholds $S_{\nu,\text{limt}}$ of 0.08 Jy, 7.85 Jy, and 0.11 Jy for Parkes, ASKAP, and CHIME according to Equation (4) by adopting the maximum pulse widths instead of the integration times $\Delta\tau$ of telescopes.

In particular, the sensitivities of FAST are adopted when the two following cases are taken into account here. One corresponds to a sensitivity for a maximum pulse width of $\sim$10 ms for sFRB 180301 and the other has a sensitivity for a maximum pulse width of $\sim$5.0 s for lFRB 160920. Using the Equation (9) in Zhang et al. (2015), we obtain the detection thresholds $S_{\nu,\text{limt}}$ of FAST to be 3.12 mJy for sFRBs and 0.14 mJy for lFRBs when an aperture efficiency of 0.63 (Jiang et al. 2020), an average system temperature of 24 K (Li et al. 2018; Jiang et al. 2020), a signal-to-noise ratio of 7 (Niu et al. 2021), and the entire 500 MHz bandwidth are employed. In fact, such a deep threshold has been demonstrated also in pulsar detections by FAST (e.g., Wang et al. 2021). For the ultralong FRBs detected by Pushchino Radio Astronomy Observatory, the fluctuational sensitivity in a 2.5 MHz receiver bandwidth with a time resolution of 0.1 s is taken as 140 mJy (Fedorova & Rodin 2019a, 2019b, 2021).

Figure 4 displays how peak flux density evolves with redshift. It can be seen that peak flux density will be almost independent of redshift when the distance of a given FRB is far enough. In other words, the detected event rate of FRBs will be approximately independent of redshift, which is very similar to the dependency of peak flux on redshift for the GRBs found by Zhang et al. (2018b). For comparison, we also estimate the detecting sensitivity of the Square Kilometre Array (SKA) by assuming $\Delta\tau = 3.5$ s and $\Delta\nu = 700$ MHz according to Zhang et al. (2018b). Figure 4 shows that FAST and SKA exhibit an outstanding detectability for the high-redshift FRBs, which helps us disclose the physical origins of diverse FRBs. It is necessary to be aware that the flux density of FRB host galaxies is surprisingly independent of redshift as well (Heintz et al. 2020). The consistency of flux density evolving with redshift of FRBs and their hosts are quite similar to that of GRB afterglows and their host galaxies in radio bands

(Zhang et al. 2018b), which implies that FRBs could be used as a standard candle for cosmological studies.

4. Conclusions and Discussions

Based on the above investigations, our results are summarized as follows:

1. We define our FRB samples with a central frequency below/above 1 GHz as subsample I/II, to check the frequency dependence of FRB classifications. It is found that there is a clear bimodal distribution of the W_{obs} for subsample I. We separated subsample I into sFRBs and lFRBs with a boundary of 100 ms. We find the sFRBs with a higher central frequency are shorter than those with a lower central frequency not only for nonrepeating but also for repeating sFRBs. However, the result of lFRBs is ambiguous due to a small number of samples.

2. Nonrepeating sFRBs are brighter than repeating bursts on average. A power-law relation of $F \propto S_{p,obs}^{\gamma}$ is found to exist for nonrepeating and repeating FRBs with a roughly consistent power-law index of $\gamma \sim 0.9$. However, the intercept of the F–$S_{p,obs}$ relations of lFRBs and sFRBs is largely different.

3. It is confirmed that repeating FRBs in our sample are less energetic than nonrepeating sFRBs on the whole. More importantly, we find that the averaged isotropic energy of lFRBs is larger than that of sFRBs by at least two orders of magnitude, which is surprisingly similar to the difference between short and long GRBs.

4. In terms of Figures 2 and 3, we conclude that the "one-off" events (at least part of them) at present could be repetitive in nature, which demonstrates these kinds of repeating and nonrepeating FRBs might share the same radiation mechanism. However, lFRBs and sFRBs are significantly diverse and could originate from different progenitors.

5. We have investigated the dependence of the peak flux density on the cosmological redshift and find that the peak flux density exhibits an independence of the redshift when the distance of the FRBs becomes far enough. The ongoing and upcoming large radio telescopes including FAST and SKA have significant potential to detect more and fainter FRBs at very high redshift in the near future.

In practice, there are various potential factors that misclassify a repeating FRB into an one-off source. The instrumental and analytical biases, such as the beam response and the limited time resolution, lead to some repeating bursts being unresolved and missing (e.g., Connor 2019; Pleunis et al. 2021b). In addition, the limited sensitivity of current telescopes and the absence of follow-up observations can also cause many repeating bursts to be missed (Kumar et al. 2019; Xiao et al. 2021). These questions are expected to be solved sooner or later, with high-sensitivity multiple facilities and the cumulation of observation time in the era of large telescopes.

Recently, a bright FRB 200428 was reported from a Galactic magnetar (CHIME/FRB Collaboration et al. 2020; Bochenek et al. 2020), of which the discovery confirmed that magnetars are capable of producing FRBs. Iwazaki (2021) proposed a generation mechanism from the axion star collision with compact objects to explain some differences between repeating and nonrepeating FRBs. In particular, Iwazaki (2021) proposes that the association between FRB 200428 and magnetar SGR J1935+2154 may result from the collision of an axion with the magnetar. Unfortunately, the number of FRBs produced by an established progenitor including magnetars is too limited nowadays. Therefore, our statistical results of the observed spectral–temporal properties can impose strong constraints on the generation mechanism of different kinds of FRBs.

The 11 lFRBs are all detected at the frequency range of 111 ± 2.5 MHz over six frequency channels, each with a narrow receiver bandwidth of 415 kHz (Fedorova & Rodin 2019a, 2019b). The unambiguous astrophysical origin is questioned by Pleunis et al. (2021a) because of the low frequency, the narrow receiver bandwidth, the large number of trials in their blind search, and the low S/N value of the claimed events. Meanwhile, Nikitin (2021) suggested that the effect of the interstellar scatter broadening at 111 MHz low frequency is stronger than that at higher frequencies and causes the durations of pulse to be several seconds. Fedorova & Rodin (2019b) suggested that different widths of the lFRBs cannot be explained purely by broadening in the receiver bandwidth and are also associated with internal properties of the pulses. Interestingly, Alexander & Fedorova (2020) reported an FRB with a wider pulse width of 2.2 s and a specific fluence of 308 Jy ms at an observing frequency of 111 MHz from SGR J1935+2154 detected by the Big Scanning Array of the Lebedev Physical Institute (BSA/LPI), which is interpreted as an off-beam "slow" radio burst of the on-beam FRB 200428 associated with the SGR burst by Zhang (2021). If such an interpretation is correct, the lFRBs, at least some of them, could be explained by the off-beam mechanism in a similar way. Consequently, joint observations of full electromagnetic waves (especially at low frequency) and multiple messages including gravitational waves would shed new lights on the nature of different kinds of FRBs.

ORCID iDs

Z. B. Zhang ⓘ https://orcid.org/0000-0003-4859-682X
D. Li ⓘ https://orcid.org/0000-0003-3010-7661

References

Alexander, R., & Fedorova, V. 2020, ATel, 14186, 1
Aggarwal, K. 2021, ApJL, 920, L18
Beloborodov, A. M. 2017, ApJL, 843, L26
Bennett, C. L., Larson, D., Weiland, J. L., et al. 2014, ApJ, 794, 135
Bhardwaj, M., Gaensler, B. M., Kaspi, V. M., et al. 2021, ApJL, 910, L18
Bhattacharyya, S. 2017, arXiv:1711.09083
Bochenek, C. D., Ravi, V., Belov, K. V., et al. 2020, Natur, 587, 59
Caleb, M., Flynn, C., Bailes, M., et al. 2016, MNRAS, 458, 718
Chandra, P., & Frail, D. A. 2012, ApJ, 746, 156
CHIME/FRB Collaboration, Amiri, M., Bandura, K., et al. 2019a, Natur, 566, 235
CHIME/FRB Collaboration, Amiri, M., Bandura, K., et al. 2018, ApJ, 863, 48
CHIME/FRB Collaboration, Andersen, B. C., Bandura, K., et al. 2019b, ApJL, 885, L24

CHIME/FRB Collaboration, Andersen, B. C., Bandura, K. M., et al. 2020, Natur, 587, 54
Cho, H., Macquart, J.-P., Shannon, R. M., et al. 2020, ApJL, 891, L38
Connor, L. 2019, MNRAS, 487, 5753
Dai, Z. G. 2020, ApJL, 897, L40
Dai, Z. G., & Zhong, S. Q. 2020, ApJL, 895, L1
Dai, Z. G., Wang, J. S., Wu, X. F., et al. 2016, ApJ, 829, 27
Deng, C.-M., Wei, J.-J., & Wu, X.-F. 2019, JHEAp, 23, 1
Dong, Y.-Z., Gu, W.-M., Liu, T., et al. 2018, MNRAS, 475, L101
Falcke, H., & Rezzolla, L. 2014, A&A, 562, A137
Fedorova, V. A., & Rodin, A. E. 2019a, ARep, 63, 39
Fedorova, V. A., & Rodin, A. E. 2019b, ARep, 63, 877
Fedorova, V. A., & Rodin, A. E. 2021, ARep, 65, 776
Fonseca, E., Andersen, B. C., Bhardwaj, M., et al. 2020, ApJL, 891, L6
Gajjar, V., Siemion, A. P. V., Price, D. C., et al. 2018, ApJ, 863, 2
Geng, J. J., & Huang, Y. F. 2015, ApJ, 809, 24
Geng, J. J., Li, B., & Huang, Y. F. 2021, Innov, 2, 100152
Gu, W.-M., Dong, Y.-Z., Liu, T., et al. 2016, ApJL, 823, L28
Heintz, K. E., Prochaska, J. X., Simha, S., et al. 2020, ApJ, 903, 152
Huang, Y. F., & Geng, J. J. 2016, in ASP Conf. Ser. 502, Frontiers in Radio
    Astronomy and FAST Early Sciences Symposium 2015, ed. L. Qain &
    D. Li (San Francisco, CA: ASP), 1
Iwazaki, A. 2021, PhRv, D104, 043022
Jiang, P., Tang, N.-Y., Hou, L.-G., et al. 2020, RAA, 20, 064
Josephy, A., Chawla, P., Fonseca, E., et al. 2019, ApJL, 882, L18
Kashiyama, K., Ioka, K., & Mészáros, P. 2013, ApJL, 776, L39
Kass, R., & Raftery, A. 1995, J. Am. Stat. Assoc., 90, 773
Kumar, P., Shannon, R. M., Osłowski, S., et al. 2019, ApJL, 887, L30
Li, B., Li, L.-B., Zhang, Z.-B., et al. 2019, Int. J. Cosmol. Astron. Astrophys.,
    1, 22, arXiv:1901.03484
Li, D., Wang, P., Qian, L., et al. 2018, IMMag, 19, 112
Li, D., Wang, P., Zhu, W. W., et al. 2021, Natur, 598, 267
Lorimer, D. R., Bailes, M., McLaughlin, M. A., et al. 2007, Sci, 318, 777
Luo, R., Wang, B. J., Men, Y. P., et al. 2020, Natur, 586, 693
Lyubarsky, Y. 2014, MNRAS, 442, L9
Lyutikov, M., Burzawa, L., & Popov, S. B. 2016, MNRAS, 462, 941

Masui, K., Lin, H.-H., Sievers, J., et al. 2015, Natur, 528, 523
Metzger, B. D., Margalit, B., & Sironi, L. 2019, MNRAS, 485, 4091
Michilli, D., Seymour, A., Hessels, J. W. T., et al. 2018, Natur, 553, 182
Mingarelli, C. M. F., Levin, J., & Lazio, T. J. W. 2015, ApJL, 814, L20
Nikitin, I. 2021, JPhCS, 1730, 012073
Niu, C.-H., Li, D., Luo, R., et al. 2021, ApJL, 909, L8
Pedregosa, F., Varoquaux, G., Varoquaux, A., et al. 2011, J. Mach. Learn.
    Res., 12, 2825
Petroff, E., Barr, E. D., Jameson, A., et al. 2016, PASA, 33, e045
Platts, E., Weltman, A., Walters, A., et al. 2019, PhR, 821, 1
Pleunis, Z., Michilli, D., Bassa, C. G., et al. 2021a, ApJL, 911, L3
Pleunis, Z., Good, D. C., Kaspi, V. M., et al. 2021b, arXiv:2106.04356
Price, D. C., Foster, G., Geyer, M., et al. 2019, MNRAS, 486, 3636
Scholz, P., Spitler, L. G., Hessels, J. W. T., et al. 2016, ApJ, 833, 177
Shannon, R. M., Macquart, J.-P., Bannister, K. W., et al. 2018, Natur,
    562, 386
Soderberg, A. M., Kulkarni, S. R., Berger, E., et al. 2004, ApJ, 606, 994
Spitler, L. G., Scholz, P., Hessels, J. W. T., et al. 2016, Natur, 531, 202
Sun, H., Niu, G. C., Shen, M. L., et al. 2021, in preparation
Tarnopolski, M. 2016, NewA, 46, 54
Thornton, D., Stappers, B., Bailes, M., et al. 2013, Sci, 341, 53
Totani, T. 2013, PASJ, 65, L12
Wang, P., Li, D., & Clark, C. 2021, CPMA, 64, 129562
Xiao, D., Wang, F., & Dai, Z. 2021, SCPMA, 64, 249501
Xu, S. Y., & Zhang, B. 2016, ApJ, 832, 199
Zhang, B. 2014, ApJL, 780, L21
Zhang, B. 2017, ApJL, 836, L32
Zhang, B. 2018a, ApJL, 867, L21
Zhang, B. 2018b, ApJL, 854, L21
Zhang, B. 2020a, Natur, 587, 45
Zhang, B. 2021, ApJL, 907, L17
Zhang, Z. B., Kong, S. W., Huang, Y. F., et al. 2015, RAA, 15, 237–51
Zhang, Z. B., Yang, E. B., Choi, C. S., et al. 2016, MNRAS, 462, 3243
Zhang, Z. B., Zhang, C. T., Zhao, Y. X., et al. 2018a, PASP, 130, 054202
Zhang, Z. B., Chandra, P., Huang, Y. F., et al. 2018b, ApJ, 865, 82
Zhu, W. W., Li, D., Luo, R., et al. 2020, ApJL, 895, L6